Fractal heterogeneous media

Christian Türk,[1,*] Anna Carbone,[1,†] and Bernardino M. Chiaia[2,‡]
[1]*Physics Department and CNISM, Politecnico di Torino, Corso Duca degli Abruzzi 24, I-10129 Torino, Italy*
[2]*Department of Structural and Geotechnical Engineering, Politecnico di Torino, Corso Duca degli Abruzzi 24, I-10129 Torino, Italy*
(Received 4 December 2009; revised manuscript received 19 January 2010; published 17 February 2010)

A method is presented for generating compact fractal disordered media by generalizing the random midpoint displacement algorithm. The obtained structures are *invasive stochastic fractals*, with the Hurst exponent varying as a continuous parameter, as opposed to *lacunar deterministic fractals*, such as the Menger sponge. By employing the detrending moving average algorithm [A. Carbone, Phys. Rev. E **76**, 056703 (2007)], the Hurst exponent of the generated structure can be subsequently checked. The fractality of such a structure is referred to a property defined over a three-dimensional topology rather than to the topology itself. Consequently, in this framework, the Hurst exponent should be intended as an estimator of *compactness* rather than of *roughness*. Applications can be envisaged for simulating and quantifying complex systems characterized by self-similar heterogeneity across space. For example, exploitation areas range from the design and control of multifunctional self-assembled artificial nanostructures and microstructures to the analysis and modeling of complex pattern formation in biology, environmental sciences, geomorphological sciences, etc.

DOI: 10.1103/PhysRevE.81.026706 PACS number(s): 05.10.−a, 05.45.Df, 61.43.−j, 62.23.St

I. INTRODUCTION

Real world materials, such as stable and metastable liquids, glasses, defective crystals, and structures that evolve from nonequilibrium processes, always exhibit a certain degree of disorder. On the other hand, the design of artificial heterogeneous structures and the accurate control of their structural, chemical or orientational disorder is an area of intensive investigation for fundamental and technological interest [1–13]. Recent developments in nanophotonics have shown that it is possible to make use of the intrinsic disorder in natural and photonic materials to create new optical structures and functionalities [14]. Fractal bodies, such as Menger sponges [15], have demonstrated the ability to perform novel functions as localize electromagnetic and acoustic waves [16–18] or enhance superliquid repellency or dewettability [19,20]. The reconstruction of heterogeneous media, from the knowledge of the correlation function, is a challenging inverse problem. Any reconstruction procedure requires to be effectively controlled in order to enable the prediction, design, and implementation of structures exhibiting the desired electromagnetic, transport, or biological functions [21–28].

The disorder degree of a medium can be quantified in terms of the two-point correlation function $C(\mathbf{r}_1,\mathbf{r}_2)=\langle f(\mathbf{r}_1)f(\mathbf{r}_2)\rangle$ of a relevant quantity $f(r)$ (e.g., dielectric function, porosity, density), where $\mathbf{r}_1,\mathbf{r}_2$ are two arbitrary points in the system. For statistically isotropic media, $C(\mathbf{r}_1,\mathbf{r}_2)$ depends only on the distance $\lambda=\|\mathbf{r}_2-\mathbf{r}_1\|$ between two points; thus, it is written as $C(\lambda)$. For fully uncorrelated systems, such as the ideal gas, the correlation function is a simple exponential, $C(\lambda)\propto\exp(-\lambda/a)$, while for fully ordered media, such as the perfect lattice, the correlation function $C(\lambda)$ is a constant. Generally, heterogeneous materials exhibit forms of correlation which are intermediate between those of the ideal gas and the perfect lattice.

Fractional Brownian functions are characterized by a correlation function depending as a power law on λ [29,30]. Such a correlation may reasonably account for the intermediate behavior, between the fully uncorrelated exponential and the fully correlated constant decay, exhibited by real disordered media. The power-law correlation of fractional Brownian functions can be expressed by the power-law dependence of the variance,

$$\langle[f_H(r+\lambda)-f_H(r)]^2\rangle=\sigma_o^2\|\lambda\|^{2H}, \tag{1}$$

with $f_H(r):\mathbb{R}^d\rightarrow\mathbb{R}$, with $r=(x_1,x_2,\ldots,x_d)$, $\lambda=(\lambda_1,\lambda_2,\ldots,\lambda_d)$, and $\|\lambda\|=\sqrt{\lambda_1^2+\lambda_2^2+\cdots+\lambda_d^2}$. H is the Hurst exponent, which is related to the fractal dimension through the relation $D=d+1-H$, with d the embedded Euclidean dimension. H ranges from 0 to 1, taking the values $H=0.5$, $H>0.5$, and $H<0.5$ respectively for uncorrelated, correlated and anticorrelated Brownian functions.

Concepts such as scaling, criticality, and fractality have been proven useful to model dynamic processes; stress-induced morphological transformation; isotropic and anisotropic fracture surfaces; static friction between materials dominated by hard-core interactions; elastic and contact properties; diffusion and transport in porous and composite materials; mass fractal features in wet/dried gels, liposome, and colloids; physiological organs (e.g., lung); and polarizabilities, hydrophobicity of surfaces with hierarchic structure undergoing natural selection mechanism and solubility of nanoparticles. Several quantification methods have been proposed to accomplish accurate and fast estimates of power-law correlations at different scales [31–44].

In the present work (1) a compact invasive stochastic fractal structure is obtained by generalizing the random midpoint displacement (RMD) algorithm to high dimension (Sec. II). In topological dimension $d=3$, a fractal cube with size $N_1\times N_2\times N_3$ is obtained, whose relevant property (e.g.,

*christian.turk@polito.it
†anna.carbone@polito.it
‡bernardino.chiaia@polito.it

density, dielectric function, porosity) is described as a three-dimensional fractional Brownian field $f_H(r)$. As opposed to deterministic lacunar fractals, such as the Menger sponge whose fractal dimension is equal to 2.7268, the obtained medium is a stochastic invasive fractal. By varying the Hurst exponent, which is given as input of the algorithm, between 0 and 1, the fractal dimension D is continuously varied between $D=3$ and $D=4$. It is worthy of remark that in this case the fractal dimension D refers to the *compactness* rather than to *roughness* as in the case of fractal surfaces and interfaces. Such a structure can be used for describing complex materials with correlation function exhibiting a power-law dependence over distance and arbitrary degree of heterogeneity expressed by H.

(2) The degree of disorder of the medium is quantified in terms of the Hurst exponent, whose estimate is provided by the detrended moving average (DMA) algorithm [34] (Sec. III). The algorithm calculates the generalized variance $\sigma_{DMA}(s)$ of the fractional Brownian fields $f_H(r)$ around the three-dimensional moving average function $\tilde{f}_H(r,s)$. The generalized variance $\sigma_{DMA}(s)$ is estimated over subcubes with size $n_1 \times n_2 \times n_3$ and, then, summed over the whole domain $N_1 \times N_2 \times N_3$ of the fractal cube. The value of $\sigma_{DMA}(s)$ for each subcube is then plotted in log-log scale as a function of $s=\sqrt{n_1^2+n_2^2+n_3^2}$. The linearity of this plot guarantees the power-law dependence of the correlation over the investigated range of scales. The slope of the plot yields the Hurst exponent H of the fractional Brownian field.

II. GENERATION OF COMPLEX HETEROGENEOUS MEDIA

The random midpoint displacement algorithm is a recursive technique widely used for generating fractal series and surfaces. In $d=1$, a fractional Brownian walk is obtained starting from a line of length N. At each iteration j, the value at the midpoint is calculated as the average of the two end points plus a correction which scales as the inverse of the length of half segment with exponent H. The fractal dimension is $D=2-H$, varying between 1 and 2. Fractal surfaces with desired roughness can be generated starting from a plane, whose domain is a regularly spaced square lattice with size $N_1 \times N_2$, $i_1=1,2,\ldots,N_1$, and $i_2=1,2,\ldots,N_2$. First, the square is divided in four subsquares. Then, the value in the center of the square is calculated as the average of the values at the four vertices plus a random term. Then, the four values at the midpoint of the edges are obtained as the average of the values at the two adjacent vertices plus a random term. The process is repeated until the fractal surface is obtained. The fractal dimension is $D=3-H$, varying between 2 and 3. Here, a high-dimensional implementation of the algorithm is presented for obtaining a compact body, exhibiting power-law correlation over a wide span of scales.

A. *d*-dimensional random midpoint displacement algorithm

Here, the random midpoint displacement algorithm is generalized to be operated on arrays with arbitrary Euclidean dimension d. The procedure is generalized by defining the function,

$$f_H(r) = \frac{1}{2^d}\sum_k f_k(r) + \sigma_{j,d}, \tag{2}$$

which is defined at the center of a hypercubic equally spaced lattice. The sum is calculated over the k end points of the lattice. The explicit expression of the quantity $\sigma_{j,d}$ at each iteration j is worked out below. We start from Eq. (1), that is written as

$$\langle [f_H(r+\lambda) - f_H(r)]^2 \rangle = \sigma_o^2 (\sqrt{\lambda_1^2 + \lambda_2^2 + \cdots + \lambda_d^2})^{2H}, \tag{3}$$

by considering a hypercubic lattice with size $N_1=N_2=\cdots=N_d=N$, Eq. (3) is written as

$$\langle [f_H(r+N) - f_H(r)]^2 \rangle = \sigma_o^2 (\sqrt{d}N)^{2H}. \tag{4}$$

By dividing each lattice size by a factor 2 at each iteration, Eq. (4) is rewritten as

$$\left\langle \left[f_H\left(r + \frac{N}{2^j}\right) - f_H(r) \right]^2 \right\rangle = \sigma_o^2 \left(\frac{\sqrt{d}N}{2^j} \right)^{2H}. \tag{5}$$

Moreover, at each iteration, the following relation holds:

$$\left\langle \left[f_H\left(r + \frac{N}{2^j}\right) - f_H(r) \right]^2 \right\rangle = \frac{1}{4^d} \left\langle \left[f_H\left(r + \frac{N}{2^{j-1}}\right) - f_H(r) \right]^2 \right\rangle + \sigma_{j,d}^2, \tag{6}$$

being the value of $f_H(r)$ at each step of the algorithm calculated over two points for $d=1$ (extremes of a segment), four points for $d=2$ (vertices of a square), eight points for $d=3$ and so on. By using Eq. (5), Eq. (6) becomes

$$\sigma_o^2 \left(\frac{\sqrt{d}N}{2^j} \right)^{2H} = \frac{\sigma_o^2}{4^d} \left(\frac{\sqrt{d}N}{2^{j-1}} \right)^{2H} + \sigma_{j,d}^2, \tag{7}$$

and the term $\sigma_{j,d}^2$ is written as

$$\sigma_{j,d}^2 = \sigma_o^2 \left(\frac{\sqrt{d}N}{2^j} \right)^{2H} [1 - 2^{2(H-d)}], \tag{8}$$

which is the generalized form of the relationship holding for $d=1$ [45].

B. Three-dimensional media

Here, Eqs. (2) and (8) are used to yield a compact random fractal with embedded Euclidean dimension $d=3$. As already stated, the relevant property of the disordered medium is defined by the scalar function $f_H(r):\mathbb{R}^3 \to \mathbb{R}$, with $r=(x_1,x_2,x_3)$. To generate the fractal structure, a cubic array with size $N_1 \times N_2 \times N_3$ is defined. Initially, the cube is fully homogeneous with the function describing the fractal property of the medium is taken as a constant, e.g., $f_H(r)=0$.

Then, the algorithm is implemented at each iteration j according to the following steps:

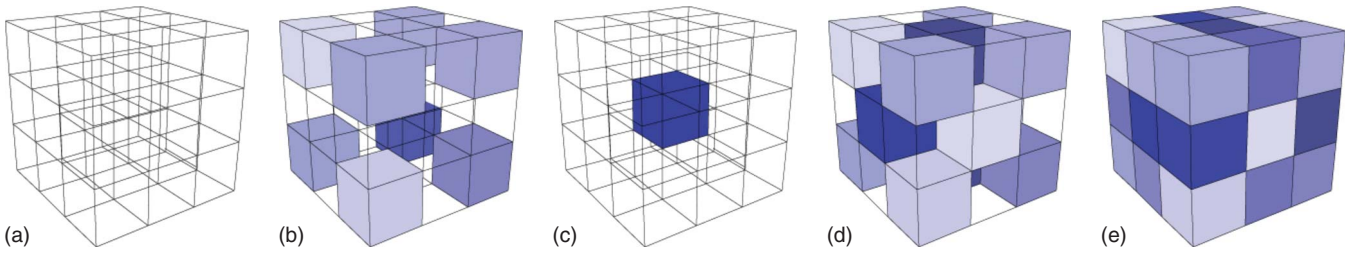

FIG. 1. (Color online) Scheme of the elementary steps of the implementation described in Sec. II. Step 1: the homogeneous cube is divided in 27 subcubes (a). Step 2: the function is calculated at the subcubes located at the eight vertices (b). Step 3: the function is calculated at the subcube located in the center (c). Step 4: the function is calculated at subcubes located at the center of the six faces (d). Step 5: the function is calculated at the subcubes located at the midpoint of the 12 edges.

(i) Step 1. The cube is divided in 27 subcubes, as shown in Fig. 1(a).

(ii) Step 2. The values of the function $f_{H,j}(r)$ are seeded as random variables of average value 0 and standard deviation $\sigma_{j,3}$ at the eight subcubes located at the eight vertices, as shown in Fig. 1(b):

(iii) Step 3. The values of the function $f_{H,j}(r)$, at the central subcube, are calculated as follows:

$$f_{H,j}(r) = \frac{1}{8}\sum_{k=1}^{8} f_k(r) + \sigma_{j,3}, \tag{9}$$

where the sum is performed over the k-values taken by the function $f(r)$ at the subcubes located at the eight vertices of the main cube. The quantity $\sigma_{j,3}$ satisfies the relation

$$\sigma_{j,3}^2 = \sigma_o^2\left(\frac{\sqrt{3}N}{2^j}\right)^{2H}[1 - 2^{2(H-3)}]. \tag{10}$$

(iv) Step 4. The values of the function $f_{H,j}(r)$, defined over the subcubes located at the center of the six faces, are calculated as follows:

$$f_{H,j}(r) = \frac{1}{4}\sum_{k=1}^{4} f_k(r) + \sigma_{j,2}, \tag{11}$$

where the sum is performed over the k-values taken by the function $f_{H,j}(r)$ at the subcubes placed at the four vertices of each face. The quantity $\sigma_{j,2}$ satisfies the relation

$$\sigma_{j,2}^2 = \sigma_o^2\left(\frac{\sqrt{2}N}{2^j}\right)^{2H}[1 - 2^{2(H-2)}]. \tag{12}$$

(v) Step 5. The values of the function $f_{H,j}(r)$ at the subcubes located at the midpoint of the twelve edges, are calculated according to

$$f_{H,j}(r) = \frac{1}{2}\sum_{k=1}^{2} f_k(r) + \sigma_{j,1}, \tag{13}$$

where the sum is performed over the k values taken by the function $f(r)$ at the subcubes located at the end points of the 12 edges. The quantity $\sigma_{j,1}$ satisfies the relation

$$\sigma_{j,1}^2 = \sigma_o^2\left(\frac{N}{2^j}\right)^{2H}[1 - 2^{2(H-1)}]. \tag{14}$$

Hence, the function $f_{H,j}(r)$ at the subcubes located at the midpoint of each edge takes a value given by the average of the function at the end-point subcubes plus the quantity $\sigma_{j,1}$.

The first run of the routine results in 27 subcubes, characterized by the values of the function $f_H(r)$ described above. The structure obtained at the first iteration is shown in Fig. 1(e). The steps 1–5 are iteratively repeated for each of the 27 subcubes. At the second run, a number of subcubes equal to 27×27 are obtained. Eventually, the number of subcubes will be equal to $(3^j)^d$, where j is the iteration number and $d=3$.

In Fig. 2, the fractal cubes with Hurst exponent (a) $H=0.2$, (b) $H=0.5$, and (c) $H=0.8$, and fractal dimension (a) $D=3.8$, (b) $D=3.5$, and (c) $D=3.2$ are shown at iteration $j=9$. The Hurst exponent is the input of the generator, which determines the heterogeneity of the resulting microstructure. The color map is rescaled in such a way that the lightest cubes correspond to the value of $f_H(r)$ at the initial stage of the medium, darker dots to the maximum values obtained by applying the routine to the function $f_H(r)$.

An alternative representation can be obtained by relating the fractional Brownian function $f_H(r)$ to the grain size. Granular structures with different Hurst exponents are shown in Figs. 3(a)–3(c). In this case, the fractal function $f_H(r)$ is referred to the size (namely, the radius) of the grains, whose shape is spherical. One can notice that, for anticorrelated granular media with $H=0.2$, small grains are more likely to

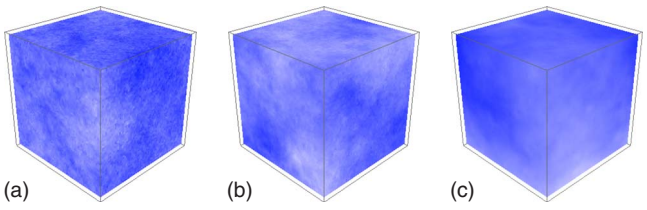

FIG. 2. (Color online) Fractal media generated according to the procedure reported in Sec. II. The Hurst exponents are, respectively, (a) $H=0.2$, (b) $H=0.5$, and (c) $H=0.8$. The fractal dimensions are, respectively, (a) $D=3.8$, (b) $D=3.5$, and (c) $D=3.2$. The color map is rescaled in order that white dots correspond to the minimum values and darkest dots to the maximum values of $f_H(r)$.

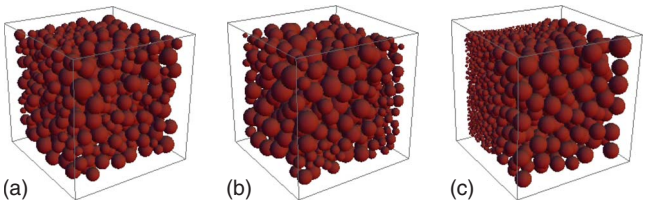

FIG. 3. (Color online) Granular structures obtained by considering spheres with radius described by the function $f_H(r)$. The Hurst exponents are, respectively, (a) $H=0.2$, (b) $H=0.5$, and (c) $H=0.8$. The fractal dimensions are, respectively, (a) $D=3.8$, (b) $D=3.5$, and (c) $D=3.2$. The average radius of the grains is equal to 2 mm. We remark that, in order to allow the visualization of the elementary grains of the media, only a limited number of grains are shown. An average number of about $10\times10\times10$ values (grains) are represented; i.e., the images correspond only to a small portion of the whole fractal cube.

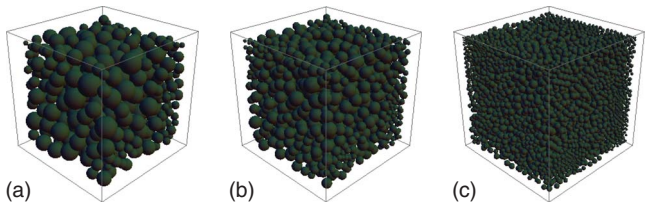

FIG. 4. (Color online) Granular structures obtained by considering spheres with the radii described by the function $f_H(r)$ with three different average grain size. The average radius of the grains is equal to (a) 2 mm, (b) 1.5 mm, and (c) 1 mm, respectively. The Hurst exponent is $H=0.5$ and the fractal dimension is $D=3.5$ for all the three cases. An average number of about $10\times10\times10$, $15\times15\times15$, and $20\times20\times20$ values (grains) are represented; i.e., the images correspond only to a small portion of the whole fractal cubes.

be close to large grains and vice versa [as shown in Fig. 3(a)]. Conversely, as the Hurst exponent increases, the grains segregate according to the size: smaller grains are more likely to be close to small grains, larger grains are more likely to be close to large grains [as shown in Fig. 3(c) for $H=0.8$]. It is worthy to recall the analogous behavior exhibited by fractional Brownian walks (time series). For negatively correlated series with $H<0.5$, positive increments are more likely to be followed by negative increments and vice versa. Conversely, in positively correlated series with $H>0.5$, positive increments are more likely to be followed by positive increments and vice versa. This corresponds to the occurrence of clustered events. For the fractal media generated here, the clustering effect is observed in the sample of Fig. 3(c). One can notice that larger grains are grouped together (clustered). Grains with smaller average sizes are grouped together (clustered) as well. We remark that, in order to allow the visualization of the elementary grains of the media, only a limited number of grains are shown: an average number of about $10\times10\times10$ values (grains) are represented in Figs. 3(a)–3(c). Thus, the images correspond only to a small portion of the whole fractal cube. Such a reduced size might give the impression that the lack of characteristic scales is not fulfilled. In particular, a bias (anisotropy) effect appears in Fig. 3(c), where a cluster of large grains occurs at the front face, while a cluster of small grains occurs at the back face. The whole size of the fractal media is $1025\times1025\times1025$ points, therefore several tenths of clusters of small or large grains are generated across the bulk rather than only a couple of clusters as it might appear from Fig. 3(c).

In Figs. 4(a)–4(c), granular fractal structures with different average grain sizes having the same Hurst exponent and fractal dimension ($H=0.5, D=3.5$) are also shown. The average radius of the grains is equal to (a) 2 mm, (b) 1.5 mm, (c) 1 mm, respectively.

III. ESTIMATING THE HURST EXPONENT OF RANDOM FRACTAL MEDIA

The aim of this section is to implement an independent measure of the Hurst exponent of the heterogeneous structure generated according to the procedure in Sec. II (shown in Figs. 2–4). The detrending moving average algorithm for estimating the Hurst exponent of fractals with topological dimension $d\geq2$ has been reported in [34]. In the present work, the algorithm will be implemented on the heterogeneous structures generated in Sec. II.

The core of the algorithm is the generalized variance $\sigma^2_{DMA}(s)$, which for a three-dimensional structure, is written as

$$\sigma^2_{DMA}(s)=\frac{1}{V}\sum_{V}[f_H(r)-\tilde{f}_{n_1,n_2,n_3}(r)]^2, \tag{15}$$

where $f_H(r)=f_H(x_1,x_2,x_3)$ is the fractional Brownian field with $i_1=1,2,\ldots,N$, $i_2=1,2,\ldots,N$, and $i_3=1,2,\ldots,N$. The function $\tilde{f}_{n_1,n_2,n_3}(r)$ is given by

$$\tilde{f}_{n_1,n_2,n_3}(r)=\frac{1}{\nu}\sum_{k_1}\sum_{k_2}\sum_{k_3}f_H(x_1-k_1,x_2-k_2,x_3-k_3), \tag{16}$$

with the size of the subcubes (n_1,n_2,n_3) ranging from (3, 3, 3) to the maximum values $(n_{1max},n_{2max},n_{3max})$. $\nu=n_1n_2n_3$ is the volume of the subcubes. The quantity $V=(N_1-n_{1max})(N_2-n_{2max})(N_3-n_{3max})$ is the volume of the fractal cube over which the averages $\tilde{f}$ are defined. As observed in [34], Eqs. (15) and (16) are defined for any geometry of the subarrays. However, in practice, subcubes with $n_1=n_2=n_3$ are computationally more suitable for avoiding spurious directionality and biases in the calculations. The generalized variance $\sigma^2_{DMA}(s)$ scales as $(n_1^2+n_2^2+n_3^2)^H$ because of the fundamental property of fractional Brownian functions [Eq. (1)].

Equations (15) and (16) correspond to the isotropic implementation of the algorithm. The isotropy follows from the definition of the average $\tilde{f}_{n_1,n_2,n_3}(r)$, which is obtained by summing all the values taken by $f_H(r)$ at the subcubes centered in r. As explained in [34], the implementation can be made anisotropic for fractals having a preferential growth direction, as for example biological tissues, epitaxial layers, crack propagation. The anisotropy is accomplished by varying the sum indexes according to $m_1=\mathrm{int}(n_1\theta_1)$, m_2

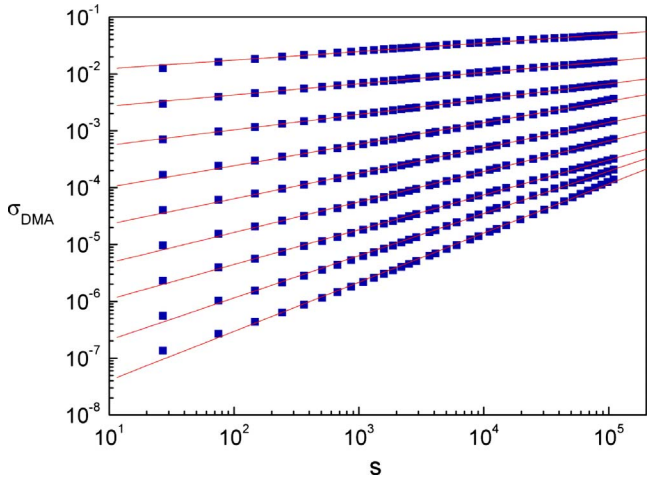

FIG. 5. (Color online) Log-log plot of $\sigma^2_{DMA}(s)$ for fractal media with size $N_1 \times N_2 \times N_3 = 1025 \times 1025 \times 1025$. The fractal media are generated by the algorithm proposed in Sec. II, with Hurst exponent varying from 0.1 to 0.9 with step 0.1. Dashed lines represent the linear fits. The Hurst exponents can be estimated by means of the 3*d*-DMA algorithm as explained in Sec. III.

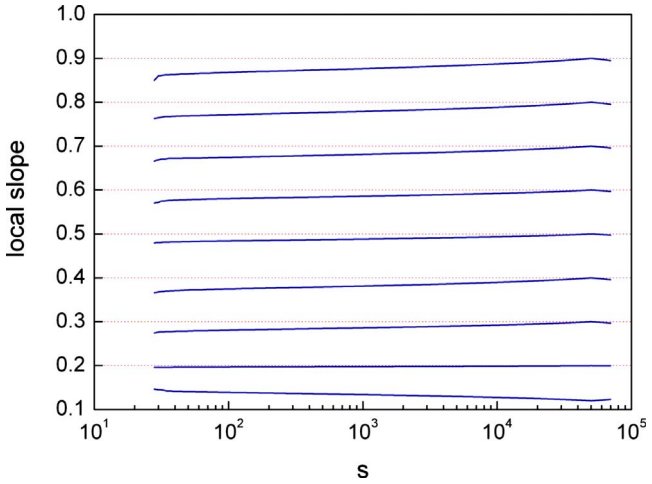

FIG. 6. (Color online) Plot of the local slopes of curves such as those shown in Fig. 5 obtained as average of ten realizations of fractal media with $N_1 \times N_2 \times N_3 = 1025 \times 1025 \times 1025$, with Hurst exponent varying from 0.1 to 0.9 with step 0.1. One can notice that the main deviations occur at the extremes of the scales.

$=\text{int}(n_2\theta_2)$, and $m_3=\text{int}(n_3\theta_3)$. Upon variation in the parameters θ_1, θ_2, and θ_3 in the range $[0, 1]$ the indexes of the sums in Eqs. (15) and (16) are set within each subcube. In particular, r coincides, respectively, with (a) one of the vertices for $\theta_1, \theta_2, \theta_3 = 0$ or 1 or with (b) the center for $\theta_1 = \theta_2 = \theta_3 = 1/2$. The values $\theta_1 = \theta_2 = \theta_3 = 1/2$ correspond to the *isotropic* implementation, while $\theta_1 = \theta_2 = \theta_3 = 0$ and $\theta_1 = \theta_2 = \theta_3 = 1$ correspond to the *directed* implementation. In $d=3$, the *isotropic* implementation implies that the function defined by Eq. (16) is calculated over subcubes whose center is r. Conversely, the *anisotropic* implementation implies that the function $\tilde{f}_{n_1,n_2,n_3}(r)$ is calculated over subcubes having one of the eight vertices coinciding with r.

In order to calculate the Hurst exponent of the heterogeneous structure, the algorithm is implemented through the following steps. The function $\tilde{f}_{n_1,n_2,n_3}(r)$ is calculated over different subcubes by varying n_1, n_2, and n_3 from $3 \times 3 \times 3$ to $n_{1max} \times n_{2max} \times n_{3max}$. The maximum values n_{1max}, n_{2max}, and n_{3max} depend on the size of the whole fractal. To minimize finite-size effects, it should be $n_{1max} \ll N_1$, $n_{2max} \ll N_2$, and $n_{3max} \ll N_3$. The next step is the calculation of the difference $f_H(r) - \tilde{f}_{n_1,n_2,n_3}(r)$ in parentheses of Eq. (15) for each subcube $n_1 \times n_2 \times n_3$. For each subcube, the corresponding value of $\sigma^2_{DMA}(s)$ is calculated and finally plotted on log-log axes. The log-log plot of $\sigma^2_{DMA}(s)$ as a function of s, yields a straight line with slope H, on account of the following relationship:

$$\sigma^2_{DMA}(s) \sim (n_1^2 + n_2^2 + n_3^2)^H \sim s^H. \tag{17}$$

In Fig. 5, the log-log plots of $\sigma^2_{DMA}(s)$ vs s are shown for fractal cubes generated according to the procedure described in Sec. II. The cubes have Hurst exponents ranging from 0.1 to 0.9 with step 0.1 and size $1025 \times 1025 \times 1025$. The plots of $\sigma^2_{DMA}(s)$ as a function s are linear according to the power-law behavior expected on the basis of Eq. (17). Dashed lines

TABLE I. Hurst exponents H_1, H_2, H_3, and H_4 and linear regression coefficients ρ_1, ρ_2, ρ_3, and ρ_4 of curves such as those of Fig. 5 obtained as average of ten realizations of heterogeneous media with $N_1 \times N_2 \times N_3 = 1025 \times 1025 \times 1025$. H_1 and H_2 have been calculated by linear fit over the full range of s. H_3 and H_4 have been calculated by linear fit over the range $10^2 \le s \le 10^4$.

H	H_1	ρ_1	H_2	ρ_2	H_3	ρ_3	H_4	ρ_4
0.1	0.1503	0.9962	0.1470	0.9965	0.1520	0.9998	0.1445	0.9995
0.2	0.1973	0.9984	0.1939	0.9984	0.2005	0.9999	0.2028	0.9999
0.3	0.2700	0.9998	0.2688	0.9998	0.2738	0.9999	0.2809	0.9996
0.4	0.3780	0.9984	0.3881	0.9980	0.3718	0.9993	0.3558	0.9997
0.5	0.4467	0.9994	0.4513	0.9994	0.4514	0.9997	0.4656	0.9993
0.6	0.5362	0.9992	0.5418	0.9993	0.5494	0.9996	0.5426	0.9997
0.7	0.6129	0.9996	0.6115	0.9997	0.6349	0.9998	0.6877	0.9992
0.8	0.7430	0.9993	0.7412	0.9995	0.7741	0.9997	0.7863	0.9997
0.9	0.8645	0.9990	0.8747	0.9991	0.8650	0.9999	0.8775	0.9999

represent the linear fits, with errors and linear regression coefficients shown in Table I. Furthermore, the local slopes of the curves are plotted in Fig. 6. Deviations from the full linearity can be observed particularly at the extremes of the scale.

IV. CONCLUSIONS

We have put forward an algorithm to generate a fully compact heterogeneous medium, whose fractal dimension can be continuously varied upon varying the Hurst exponent between 0 and 1. The generation method is based on a generalization of the random midpoint displacement algorithm. In order to check the accuracy of the generator, the Hurst exponent of the fractals can be estimated by using the high-dimensional variance $\sigma^2_{DMA}(s)$ defined by Eq. (15). We envisage fruitful applications, e.g., in three-dimensional medical image analysis, where density or granularity patterns could be interpreted synthetically by means of fractal descriptors. Generally, such a structure can properly reproduce complex systems whose heterogeneity is described by correlation decaying as a power law over space. This correlation corresponds to the intermediate behavior of real structure, as opposed to the fully uncorrelated exponential decay and the fully correlated constant decay exhibited respectively by the correlation function of ideal cases such as the perfect gas and the regular lattice.

ACKNOWLEDGMENTS

We acknowledge financial support by Regione Piemonte and Politecnico di Torino. CINECA is gratefully acknowledged for CPU time at the High Performance Computing (HPC) environment.

[1] T. Lookman and P. Littlewood, MRS Bull. **34**, 822 (2009).
[2] M. Nicodemi, A. Coniglio, and H. J. Herrmann, Phys. Rev. E **59**, 6830 (1999).
[3] C. J. Gommes and J. P. Pirard, Phys. Rev. E **80**, 061401 (2009).
[4] D. T. Fullwood, B. L. Adams, and S. R. Kalidindi, J. Mech. Phys. Solids **56**, 2287 (2008).
[5] B. M. Mladek, P. Charbonneau, and D. Frenkel, Phys. Rev. Lett. **99**, 235702 (2007).
[6] L. Corte, P. M. Chaikin, J. P. Gollub, and D. J. Pine, Nat. Phys. **4**, 420 (2008).
[7] R. D. Kamien and A. J. Liu, Phys. Rev. Lett. **99**, 155501 (2007).
[8] C. Briscoe, C. Song, P. Wang, and H. A. Makse, Phys. Rev. Lett. **101**, 188001 (2008).
[9] M. Jerkins, M. Schroter, H. L. Swinney, T. J. Senden, M. Saadatfar, and T. Aste, Phys. Rev. Lett. **101**, 018301 (2008).
[10] T. O. Williams, Int. J. Solids Struct. **42**, 971 (2005); T. O. Williams and S. C. Baxter, Probab. Eng. Mech. **21**, 247 (2006).
[11] R. Hilfer, Transp. Porous Media **46**, 373 (2002); Chem. Phys. **284**, 399 (2002); C. Manwart, U. Aaltosalmi, A. Koponen, R. Hilfer, and J. Timonen, Phys. Rev. E **66**, 016702 (2002).
[12] R. A. Ketcham, J. Struct. Geol. **27**, 1217 (2005).
[13] M. A. Knackstedt, C. H. Arns, M. Saadatfar, T. J. Senden, A. Limaye, A. Sakellariou, A. P. Sheppard, R. M. Sok, W. Schrof, and H. Steininger Proc. R. Soc. London, Ser. A **462**, 2833 (2006).
[14] D. S. Wiersma, Nat. Phys. **4**, 359 (2008).
[15] The Menger sponge is obtained by dividing a cube into 27 identical cubic pieces. Then, seven cubic pieces are removed from the center of the cube and from the center of each of the six faces. The procedure is then repeated to the 20 remaining cubes. Ideally, the procedure should be repeated infinite times. The Menger sponge has fractal dimension $D=\log_{10} 20/\log_{10} 3=2.7268$ and volume decreasing at each iteration as $V_l=(20/27)^l$. The Menger sponge, at infinite iterations, is a noncompact three-dimensional fractal structure having infinite area and zero volume.
[16] M. W. Takeda, S. Kirihara, Y. Miyamoto, K. Sakoda, and K. Honda, Phys. Rev. Lett. **92**, 093902 (2004).
[17] K. Sakoda, Phys. Rev. B **72**, 184201 (2005).
[18] B. Hou, H. Xie, W. J. Wen, and P. Sheng, Phys. Rev. B **77**, 125113 (2008).
[19] H. Mayama and K. Tsujii, J. Chem. Phys. **125**, 124706 (2006).
[20] T. Minami, H. Mayama, and K. Tsujii, J. Phys. Chem. B **112**, 14620 (2008).
[21] P. Debye and A. M. Bueche, J. Appl. Phys. **20**, 518 (1949).
[22] C. L. Y. Yeong and S. Torquato Phys. Rev. E **57**, 495 (1998); **58**, 224 (1998).
[23] Y. Jiao, F. H. Stillinger, and S. Torquato, Phys. Rev. E **76**, 031110 (2007); **77**, 031135 (2008).
[24] A. Scardicchio, C. E. Zachary, and S. Torquato, Phys. Rev. E **79**, 041108 (2009); Y. Jiao, F. H. Stillinger, and S. Torquato, Proc. Natl. Acad. Sci. U.S.A. **106**, 17634 (2009).
[25] C. H. Arns, M. A. Knackstedt, and K. R. Mecke, Phys. Rev. E **80**, 051303 (2009).
[26] J. A. Quintanilla and W. M. Jones, Phys. Rev. E **75**, 046709 (2007).
[27] T. Aste, M. Saadatfar, and T. J. Senden, Phys. Rev. E **71**, 061302 (2005).
[28] M. Wang and N. Pan, Mater. Sci. Eng. R. **63**, 1 (2008).
[29] B. B. Mandelbrot and J. W. Van Ness, SIAM Rev. **104**, 422 (1968).
[30] K. Falconer, *Fractal Geometry* (Wiley, New York, 2005).
[31] J. Aguirre, R. L. Viana, and M. A. F. Sanjuan, Rev. Mod. Phys. **81**, 333 (2009).
[32] S. Pradhan, A. Hansen, and B. Chakrabarti, e-print arXiv:0808.1375, Rev. Mod. Phys. (to be published).
[33] L. Knufing, H. Schollmeyer, H. Riegler, and K. Mecke, Langmuir **21**, 992 (2005).
[34] A. Carbone, Phys. Rev. E **76**, 056703 (2007).
[35] A. Carbone and H. E. Stanley, Physica A **384**, 21 (2007).
[36] A. Carbone, G. Castelli, and H. E. Stanley, Phys. Rev. E **69**, 026105 (2004);A. Carbone and H. E. Stanley, Physica A **340**, 544 (2004).
[37] S. Arianos and A. Carbone, J. Stat. Mech.: Theory Exp.

(2009), P03037; Physica A **382**, 9 (2007).
[38] E. Koscielny-Bunde, A. Bunde, S. Havlin, H. E. Roman, Y. Goldreich, and H. J. Schellnhuber, Phys. Rev. Lett. **81**, 729 (1998).
[39] J. W. Kantelhardt, H. E. Roman, and M. Greiner, Physica A **220**, 219 (1995).
[40] S. Davies and P. Hall, J. R. Stat. Soc. **61**, 3 (1999).
[41] G. Rangarajan and M. Ding, Phys. Rev. E **61**, 4991 (2000).
[42] P. Kestener and A. Arneodo, Stochastic Environ. Res. Risk Assess. **22**, 421 (2008); Phys. Rev. Lett. **91**, 194501 (2003).
[43] J. Alvarez-Ramirez, J. C. Echeverria, I. Cervantes, and E. Rodriguez, Physica A **361**, 677 (2006).
[44] G. F. Gu and W. X. Zhou, Phys. Rev. E **74**, 061104 (2006); W.-X. Zhou and D. Sornette, Int. J. Mod. Phys. C **13**, 137 (2002).
[45] R. H. Voss, in *Fundamental Algorithm for Computer Graphics*, edited by R. A. Earnshaw, NATO ASI Series (Springer-Verlag, Berlin, 1985), Vol. F17.